J Solid State Electrochem (2014) 18:411–425
DOI 10.1007/s10008-013-2165-5

ORIGINAL PAPER

The surface characterization and corrosion resistance of 11 % Cr ferritic/martensitic and 9–15 % Cr ODS steels for nuclear fuel reprocessing application

S. Ningshen · M. Sakairi · K. Suzuki · S. Ukai

Received: 27 March 2013 / Revised: 30 May 2013 / Accepted: 23 June 2013 / Published online: 3 August 2013

Abstract In spent fuel nuclear reprocessing plant, nitric acid is the main medium used in PUREX method. The passive film compositions and corrosion resistance of 11 % Cr ferritic/martensitic and 9–15 % Cr oxide dispersion strengthened steels in different nitric acid concentrations were studied. The open circuit potential is shifted toward more noble potential as the concentrations increased from 1 M HNO_3 to 9 M HNO_3 in all the investigated alloy steels. The results of the potentiodynamic polarization plots also exhibited a shift in corrosion potential as the concentrations increased from 1 M to 9 M HNO_3. This shift is undesirable because of risk of overshooting the potential beyond passive region and may result into transpassive corrosion. The X-ray photoelectron spectroscopy results of the passive film analysis are composed mostly of Fe_2O_3, Cr_2O_3, and Y_2O_3, and the depth profile of Fe and Cr concentrations vary depending upon the nitric acid concentration. The surface morphology after the corrosion test does not show intergranular corrosion attack at the nitric acid concentrations studied. It is desirable that materials for use in nitric acid service are resistant to such corrosion induced degradation.

Keywords F/M steel · ODS steel · Nitric acid · Passive film · Corrosion resistance

S. Ningshen
Corrosion Science and Technology Group, Indira Gandhi Centre for Atomic Research, Kalpakkam 603 102, India

S. Ningshen (✉) · M. Sakairi · K. Suzuki · S. Ukai
Faculty of Engineering, Hokkaido University, Kita-13, Nishi-8, Kita-ku, Sapporo 060-8628, Japan
e-mail: sningshen@gmail.com

S. Ningshen
e-mail: ning@igcar.gov.in

Introduction

Reduced activation martensitic ferritic (RAFM) steels with Cr content of 9–12 wt%, oxide dispersion strengthened (ODS), and ferritic/martensitic (F/M) steels are an important class of engineering materials that have received much interest in the recent years [1, 2]. These alloy steels are promising candidate materials for future nuclear power plants of fission, fusion, and hybrid reactors [3–5], and being presently explored as material for spent nuclear fuel reprocessing plants [4, 5]. The major issues of reactor materials are their service temperature performance, as the efficiency of nuclear power plants is strongly dependent upon the operating temperature. The upper operating temperature limits for conventional RAFM steels are about 550 °C [6, 7]. To counterbalance the poor mechanical properties at high temperatures of the F/M steels, ODS steels have been developed using homogeneously dispersed nanoscale oxide particles of Y–Ti–O and Ti–O [3, 6]. These oxide particles improved the thermophysical and mechanical properties at a higher temperature and thereby increase the operating temperature and higher burn-up [3, 7]. As examples, the ODS martensitic steels (7–10 % Cr) exhibited excellent creep properties up to 800 °C; beyond this temperature, the strength properties deteriorate due to the phase transformation [1, 6, 7]. Similarly, the higher chromium (14–18 % Cr) ferritic ODS steels can be used up to 1,100 °C [3, 6, 7]. The other advantages of ODS steels include void and swelling resistance [6, 7], low thermal expansion coefficient [3, 6], high thermal conductivity [3, 7], and resistance to helium embrittlement and compatibility with major cooling and breeding materials [2, 6, 7].

In spent fuel nuclear reprocessing plants, nitric acid is used in various conditions and concentrations from dilute (1–4 M) to concentrated (10–14 M), room temperature (liquid/solvent extraction) to intermediate (warm, waste

storage tanks) and to boiling temperature (dissolver, evaporator, etc.) [8, 9]. However, in the presence of oxidizing ions and boiling nitric acid stainless steels suffered severe intergranular corrosion (IGC), even if the steel is not sensitized. IGC of stainless steels in nitric acid is not due to impoverishment of chromium in the grain boundaries, and this was attributed to the transpassive corrosion [5, 8, 9]. Pure metals and the alloys of Ti, Ti–5 % Ta, Ti–5 % Ta–1.8 % Nb, Zr, etc. [8, 9] are considered as alternate to austenitic stainless steels, and recently, ODS steels have been also investigated for such an application [4, 5]. The ODS steels are known to show better corrosion resistance than the conventional ferritic–martensitic alloy steels [5, 10]. In studies carried out in hot nitric acid, higher Cr alloy of 18Cr–1W–Ti ODS steel was found to be more corrosion resistance than 14Cr–1W–Ti ferritic and 9Cr–1W–Ti martensitic ODS alloys, attributed to the higher chromium content in the passive oxide layer [5]. Similarly, in comparison between 16 % Cr ODS steels with or without Al, addition of Al was found to be beneficial in 1 M HNO_3 [4]. During different stages of the spent fuel dissolution by PUREX process, nitric acid of various concentrations is used, and thereby, the cladding material can undergo different forms of corrosion attack. The development of cladding materials is a key issue to achieve efficient and high burn-up operation of Generation IV nuclear energy systems. The benefit of ODS alloy steels as cladding material for fast breeder reactors (FBRs) was recognized in the late 1960s [7, 11]. More recently, F/M steels with 9–12 % Cr and ODS steels have been explored as an alternative to the standard austenitic stainless steels for future advanced FBR cladding and structural materials [2, 5, 7]. An advantage of the F/M steels is that it can be made in reduced activation compositions to achieve higher thermal efficiency [3, 6, 7] and exhibit a low swelling resistance under irradiation due to the body-center cubic crystal structure [3, 5]. Furthermore, to counterbalance the relatively poor mechanical properties at the high temperatures, the F/M steels are oxide dispersed strengthened to improve the mechanical properties at elevated temperatures and resistance enough to neutron irradiation embrittlement [6, 7]. Thus, an understanding of the surface morphology and corrosion resistance of F/M and ODS steels in different nitric acid media is of considerable importance, and this have been attempted in the present work.

Material and experimental methods

Materials and specimen preparation

The chemical composition of F/M and ODS steels used in the present work is listed in Table 1. The alloy steels used in this work are experimental steel grades produced for this work and not commercial grades. The ODS alloy steels are produced by powder metallurgy route and F/M steel by melting and casting. The production of ODS steels involves many processes steps, such as mechanical alloying, degassing, canning, hot extrusion, and heat treatments [1, 2, 7, 12]. For manufacturing of 9 % Cr ODS and 15 % Cr ODS steels, metallic alloyed powders and yttria (Y_2O_3) powders were mechanically alloyed, and these powders were consolidated by hot extrusion at 1150 °C. At the final heat treatment, normalizing at 1050 °C for 1 h and tempering at 800 °C for 1 h for 9 % Cr ODS steel. The 9 % Cr ODS steel structure is composed of a tempered martensite and a small amount of ferrite. Since the 15 % Cr ODS steel was heat treated and annealed at 1150 °C for 1 h, its structure is a full ferrite with the grain size of a few micrometers. The detailed on the fabrication/manufacturing process of ODS steels, its microstructure, and grain structure has been described elsewhere [1, 2, 13]. The F/M steel was manufactured by the conventional process: vacuum melting, hot forging, and hot rolling. The final heat-treatment was done by normalizing at 1,100 °C for 10 min and tempering at 1,053 °C for 1 h; the microstructure contains the tempered martensite and a small amount of ferrite.

The steel specimens were cut and abraded up to 1,000 grit SiC paper on all sides prior to mounting in an epoxy resin, using a brass rod as an electrical connection. The epoxy-mounted specimens were then abraded up to 1,000 grit SiC paper finish again, ultrasonically cleaned in acetone, and used for the corrosion experiment.

Electrochemical measurements for corrosion studies

The variation in open circuit potential (OCP) was measured at different nitric acid concentrations of 1, 3, 6, and 9 M

Table 1 Chemical composition of the alloy steels in weight percent

Steel	Cr	Ni	C	Si	Ti	W	Al	Mo	Zr	Y_2O_3	Fe
9 % Cr ODS	8.95	0.03	0.14	0.06	0.23	1.96	–	–	–	0.36	Balance
11 % Cr F/M	10.52	0.50	0.15	0.039	0.50	1.81	–	0.40	–	–	Balance
15 % Cr ODS	15.15	0.04	0.03	0.02	0.12	1.90	4.00	–	0.57	0.33	Balance

HNO_3. All the electrolytic solutions were prepared using analytical reagent grade. The samples were allowed to stabilize under an open circuit condition for 30 min, and subsequently, the OCP was measured as a function of time up to 60 min. The potentiodynamic anodic polarization experiments were carried out in different nitric acid concentrations of 1, 3, 6, and 9 M HNO_3 at room temperature using HABF5001 potentiostat (Hokuto Denko, Japan). A sample (working electrode) surface of 1 cm^2 area and flat cell volume of 300 ml was employed to contain the electrolyte and used in the corrosion experiment. The electrochemical corrosion cell consisted of three electrodes: reference Ag/AgCl (in saturated KCl) electrode, platinum counter electrode, and the working electrode (sample). The electrode potential was anodically scanned at a scan rate of 0.167 mV s^{-1} until the potential at which breakdown occurred. The starting potential for polarization curves was at 100 or 200 mV below the stable OCP. This is to ensure that the active–passive behaviors are measured during the potentiodynamic anodic polarization potential measurement. The electrolytic solution was continuously purged before the start of the experiment with pure argon gas (99.999 %) to deaerate the solution, and purging was continued throughout the entire measurement period. Two or three sets tests were conducted in each experimental condition, and all the open circuit potential and anodic polarization plots were highly reproducible. The error estimates are provided with a standard deviation value in Table 2.

Surface morphology and characterization of passive film compositions

The surface morphology of the specimens after the corrosion test was observed with a scanning electron microscopy (SEM), JEOL JSM-6510LA model. The SEM images were acquired using an acceleration voltage of 10–20 kV, and a working distance was maintained between 10 and 15 mm. Load current was maintained in 60–70 μA, and the spot size was adjusted to 40–70.

Table 2 Potentiodynamic anodic polarization test parameters obtained for 9 % Cr ODS, 11 % Cr F/M, and 15 % Cr ODS steels in different nitric acid concentrations

Electrolytic media	E_{corr} (V vs Ag/AgCl)	i_{pass} (A cm^{-2})	E_{BP} (V vs Ag/AgCl)
9 % Cr ODS steel			
1 M HNO_3	−0.154±0.004	$3.16\pm0.04\times10^{-6}$ (0.85 V)	1.09±0.011 ($E_{BP\text{-}1}$)
	0.395±0.005	$2.57\pm0.03\times10^{-5}$ (1.40 V)	1.61±0.005 ($E_{BP\text{-}2}$)
3 M HNO_3	−0.096±0.005 ($E_{corr\text{-}1}$) 0.161±0.003 ($E_{corr\text{-}2}$)	$4.11\pm0.06\times10^{-6}$ (0.85 V)	1.08±0.01 ($E_{BP\text{-}1}$)
	0.462±0.010 ($E_{corr\text{-}3}$)	$7.50\pm0.02\times10^{-5}$ (1.40 V)	1.61±0.01 ($E_{BP\text{-}2}$)
6 M HNO_3	0.585±0.002	$4.83\pm0.15\times10^{-6}$ (0.85 V)	1.12±0.01 ($E_{BP\text{-}1}$)
		$2.75\pm0.05\times10^{-4}$ (1.40 V)	1.63±0.01 ($E_{BP\text{-}2}$)
9 M HNO_3	0.676±0.008	$5.60\pm0.10\times10^{-6}$ (0.85 V)	1.14±0.03 ($E_{BP\text{-}1}$)
		$2.62\pm0.06\times10^{-4}$ (1.40 V)	1.63±0.01 ($E_{BP\text{-}2}$)
11 % Cr F/M steel			
1 M HNO_3	−0.195±0.005	$5.16\pm0.04\times10^{-6}$ (0.85 V)	1.08±0.01 ($E_{BP\text{-}1}$)
		$7.20\pm0.26\times10^{-5}$ (1.50 V)	1.64±0.04 ($E_{BP\text{-}2}$)
3 M HNO_3	0.465±0.005	$4.73\pm0.03\times10^{-6}$ (0.85 V)	1.06±0.02 ($E_{BP\text{-}1}$)
		$2.09\pm0.02\times10^{-4}$ (1.50 V)	1.62±0.02 ($E_{BP\text{-}2}$)
6 M HNO_3	0.737±0.011	$3.45\pm0.06\times10^{-6}$ (0.85 V)	1.09±0.015 ($E_{BP\text{-}1}$)
		$4.98\pm0.02\times10^{-6}$ (1.50 V)	1.61±0.015($E_{BP\text{-}2}$)
9 M HNO_3	0.724±0.014	$3.33\pm0.04\times10^{-6}$ 0.85 V)	1.11±0.015 ($E_{BP\text{-}1}$)
		$6.65\pm0.04\times10^{-4}$ (1.50 V	1.59±0.01 ($E_{BP\text{-}2}$)
15 % Cr ODS steel			
1 M HNO_3	0.125±0.005	$1.37\pm0.02\times10^{-6}$ (0.85 V)	1.15±0.018 ($E_{BP\text{-}1}$)
		$9.41\pm0.22\times10^{-5}$ (1.50 V)	1.73±0. 04 ($E_{BP\text{-}2}$)
3 M HNO_3	0.400±0.001	$1.42\pm0.02\times10^{-6}$ (0.85 V)	1.14±0.04 ($E_{BP\text{-}1}$)
		$6.38\pm0.61\times10^{-4}$ (1.50 V)	1.62±0.02 ($E_{BP\text{-}2}$)
6 M HNO_3	0.504±0.005	$1.66\pm0.02\times10^{-6}$ (0.85 V)	1.15±0.04 ($E_{BP\text{-}1}$)
		$2.51\pm0.19\times10^{-5}$ (1.50 V)	1.73±0.03 ($E_{BP\text{-}2}$)
9 M HNO_3	0.648±0.005	$2.38\pm0.02\times10^{-5}$ (0.85 V)	1.13±0.02 ($E_{BP\text{-}1}$)
		$4.23\pm0.03\times10^{-3}$ (1.50 V)	1.68±0.015 ($E_{BP\text{-}2}$)

X-ray photo-electron spectroscopy (XPS) measurements were carried out on each sample by potential sweep to the passive region. This was followed by holding the samples potentiostatically at the respective passive region for 60 min: 0.85 V vs Ag/AgCl for 9 % Cr and 15 % Cr ODS steels and 1.0 V vs Ag/AgCl for 11 % Cr F/M steel. This potential was chosen because it is in the passive region, thereby also insuring that much greater amount of material is dissolved prior to passivation for the accumulation at the surface [14, 15], and further, the polarizing in its passive state leads to the iron dissolution, which is contained in its passive layer [15]. The passive range current density during potentiostatic test was constant and <5 $\mu A/cm^2$ throughout the experiments for all the alloy steels. This indicated the stable film formation, and no metal dissolution has occurred during the passivation treatment. Subsequently, some samples were immersed in different nitric acid concentrations under OCP condition up to 60 min, and the samples were transferred immediately into the XPS analyzer chamber. The XPS measurements were performed using a JEOL JPS-9200 model equipped with dual X-ray source. Mg Kα (1,253.6 eV) X-ray was used to generate the photo electrons. During the experiments, the base pressure was maintained at 10^{-7} Pa. The X-ray gun was operated at 100 W (10 kV, 10 mA) with a takeoff angle θ=0°. A survey spectrum was, firstly, recorded to identify the elements present and high-resolution spectra of the following regions were recorded: oxygen (O 1 s), carbon (C 1 s), chromium (Cr 2p), iron (Fe 2p), and yttrium (Y 3d). SpecSurf XPS operating software was employed to collect and process all surveys and high-resolution spectra.

Results and discussion

Open circuit potential measurements

The measured OCP of 9 % Cr ODS, 11 % Cr F/M, and 15 % Cr ODS steels obtained at different concentrations of 1, 3, 6, and 9 M HNO_3 are shown in Figs. 1a–c. Similarly, an inset of the OCP versus nitric acid concentration plots for the different alloy steels is shown in Fig. 1. In Fig. 1a, the effects of nitric acid concentrations on 9 % Cr ODS steel show active potential in 1 M HNO_3 (−0.154 V) and 3 M HNO_3 (−0.150 V), where in 6 M HNO_3 (0.345 V) and 9 M HNO_3 (0.630 V), more noble potential is indicative. Similarly, the OCP of 11 % Cr F/M steel show active potential in 1 M HNO_3 (−0.201 V), 3 M HNO_3 (−0.052 V), and more noble potential in 6 M HNO_3 (0.485 V) and 9 M HNO_3 (0.651 V), respectively. However, in 15 % Cr ODS steel active potential is observed only in lower concentration of 1 M HNO_3 (−0.140 V), and more noble potential could be seen in 3 M HNO_3 (0.240 V), 6 M HNO_3 (0.430 V), and 9 M HNO_3 (0.600 V). The measured OCP stabilized immediately upon immersion for all the alloy steels, and this is attributable to the stable film formation. The XPS depth profile results of the alloy steels discuss to later show higher Cr concentration in 1 M HNO_3 than in 9 M HNO, and this may affect the film stability. In Fig. 1a–c, the gradual shift of OCP towards more noble potential in all the alloy steels is observed. Subsequently, as shown in the inset of Fig. 1 with the increase in concentration from 1 M HNO_3 to 9 M HNO_3, the OCP increases with increasing HNO_3 concentration. The shift in OCP is affected by the change in both anodic and cathodic reaction rates [16]. Generally, the noble OCP of the material in the passive region is an indicative of high passivating ability. However, high noble OCP in highly oxidizing solution can also indicate strong polarization and high corrosion rate. Furthermore, due to highly oxidizing nature of nitric acid at higher nitric acid mediums, this shift is undesirable because of risk of overshooting the potential beyond the passive region. Consequently, the rate of the reaction increases with increasing concentration of HNO_3 [9, 16]. This may lead to higher corrosion rates and IGC with preferential attack along grain boundaries in high-temperature and nitric acid concentrations as seen in stainless steels [5, 8, 9].

Potentiodynamic polarization studies in different nitric acid concentration

The potentiodynamic polarization plots of F/M and ODS steels obtained for different nitric acid concentrations are shown in Fig. 2a–c, respectively. The potentiodynamic polarization plots parameters such as corrosion potential (E_{corr}), passive current density (i_{pass}), and breakdown potential (E_{BP}) are detailed in Table 2. In Fig. 2a, the typical potentiodynamic polarization plot of 9 % Cr ODS steel is represented and are compared with those previously obtained from a similar alloy steel up to 6 M HNO_3 [13]. Furthermore, in Fig. 2a, the potentiodynamic polarization plots illustrating the stages of passivity, transpassive region [oxidation of Cr_2O_3 to Cr(VI)] and oxidation of solvent (water) are depicted. The breakdown potential (E_{BP}) is represented into two parts (Fig 2a), one representing the transpassive region denoted by $E_{BP\text{-}1}$ and $E_{BP\text{-}2}$ the beginning of the oxidation of the media (Table 2). Evidently, 9 % Cr ODS steel show a gradual shift in E_{corr} from −0.154 V ($E_{corr\text{-}1}$) in 1 M HNO_3 to 0.462 V ($E_{corr\text{-}3}$) in 3 M HNO_3, 0.585 V in 6 M HNO_3, and 0.676 V in 9 M HNO_3. This shift may be attributable to increase in the cathodic process [5] and that the E_{corr} increases when the concentration is higher. The reason behind the formation of primary ($E_{corr\text{-}1}$) and secondary corrosion potential ($E_{corr\text{-}2}$) has been already described elsewhere [13]. Furthermore, in Fig 2a, two corrosion current density minima in 1 M HNO_3 and, correspondingly, three corrosion potential values in 3 M HNO_3 may be

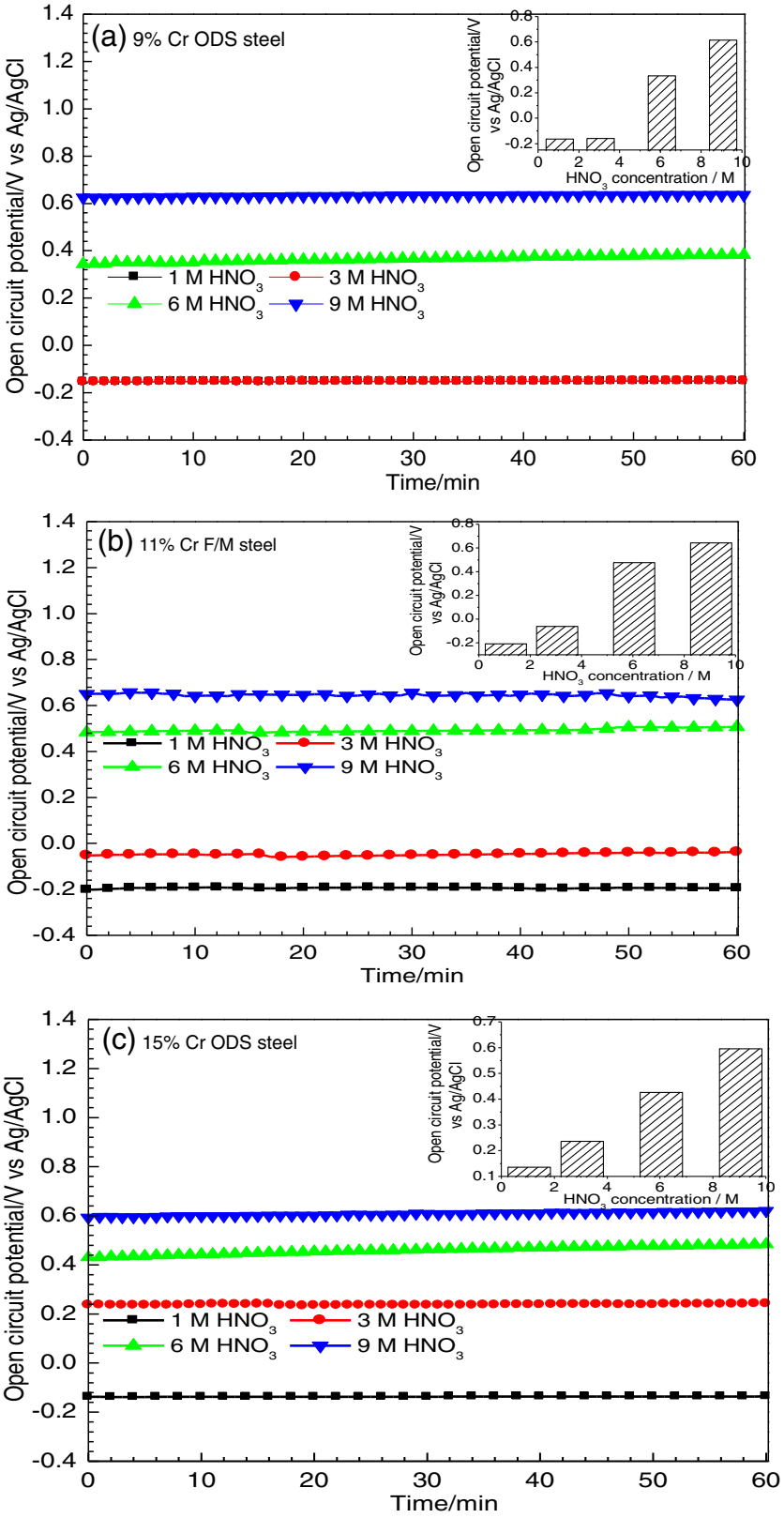

Fig 1 Open circuit potentials versus time (open circuit potentials versus HNO_3 concentration) behavior of alloy steels in different nitric acid concentrations: **a** 9 % Cr ODS steel, **b** 11 % Cr F/M steel, and **c** 15 % Cr ODS steel

attributed to incomplete passivation or the film formation process is not in the steady state. Kolman et al. [17] attributed the formation of such two to three corrosion potential in type 304L stainless steel to continuously passive, active/passive, and active surface states. Subsequently, the increased i_{pass} of 2.57×10^{-5} A cm^{-2} in 1 M HNO_3 to 2.62×10^{-4} A cm^{-2} in 9 M

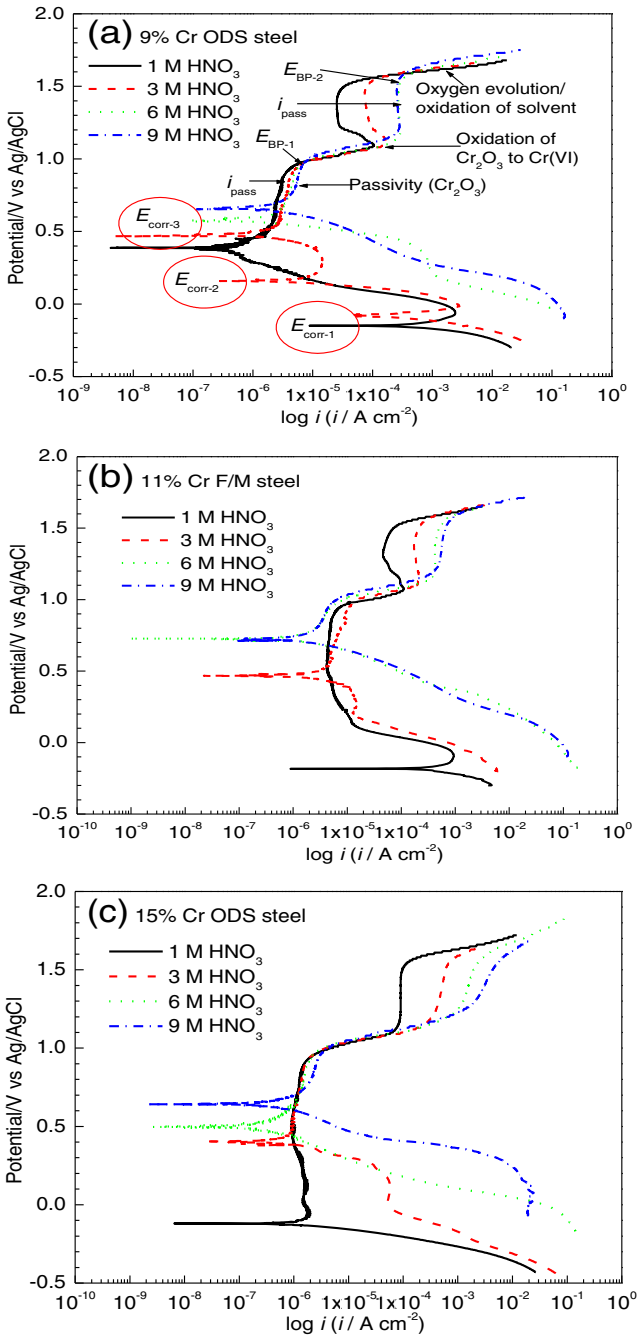

Fig 2 Potentiodynamic polarization curves of alloy steels in different nitric acid concentrations: **a** 9 % Cr ODS steel, **b** 11 % Cr F/M, and **c** 15 % Cr ODS steels

HNO_3 (Table 2) is due to the higher anodic dissolution. The potentiodynamic polarization plots of 11 % Cr F/M steel shown in Fig. 2b show shifts in E_{corr} of −0.195 V in 1 M HNO_3 to 0.465 V in 3 M HNO_3, 0.737 V in 6 M HNO_3, and 0.724 V in 9 M HNO_3. In addition, the typical potentiodynamic polarization curves of 15 % Cr ODS steel shown in Fig. 2c also shows a shift in E_{corr} from 0.125 V in 1 M HNO_3 to 0.648 V in 9 M HNO_3, and increased i_{pass} of 9.41×10^{-5} A cm^{-2} in 1 M HNO_3 to 4.23×10^{-4} A cm^{-2} in 9 M HNO_3 (Table 2). As detailed in Table 2, more active (negative) potential (−0.195 V) and nobler E_{corr} (0.724 V) was observed for 11 % Cr F/M steel followed by 9 % Cr ODS steel (−0.154 and 0.676 V) and 15 % Cr ODS steel (0.125 and 0.648 V). However, the OCP measurements in Fig. 1 and corrosion potential values from Fig. 2 (Table 2) are different, and this is expected as the method and condition of measurement are different. Thereby, the shift to higher E_{corr} as the HNO_3 concentration increase when cathodic reaction rate increases are expected based on mixed potential theory [18]. Thus, the shift of E_{corr} and OCP (Fig. 1) in the noble potential region with increased nitric acid concentration may result into transpassive corrosion. The same may hold for the ODS alloys, as a similar shift is observed. Transpassive corrosion is a phenomenon observed if the concentration and temperature increases or highly oxidizing chemical species co-exists in stainless steel and manifests itself as general corrosion with preferential attack along grain boundaries [5, 8, 19, 20]. From a practical point of view, transpassive corrosion is an important degradation mechanism induced by corrosion to the structural materials in nitric acid production plants and nuclear fuel reprocessing plants [8, 19, 24]. Furthermore, many models provide an experimental and theoretical basis for describing the breakdown/transpassive dissolution of passive film [21–23]. According to energy band model proposed by Sato [21]; the transpassive dissolution kinetic is determined by the relative positions of the Fermi level and the conduction band in the film. This model illustrates above a certain potential the passive film is electrochemically unstable, and the film dissolution rate is greater [21]. In point defect model (PDM) [22], transpassive dissolution is described in terms of mass and charge fluxes via the transport of point defects at the barrier layer interfaces. In this model, the generation and condensation of cation vacancies and annihilated by reactions leads to film decohesion and breakdown. Models presented by Bojinov et al. [23] considered two types of interfacial reactions similar to PDM to describe the formation and transpassive dissolution of the metal through the film. The transpassive dissolution reaction is assumed to be a two-stage process featuring a Cr(IV) intermediate. It also employed mathematical method and electrochemical parameters through a curve-fitting technique to explain the transpassive dissolution. The standard potential at 25 °C for the oxidation reaction from Cr(III) to Cr(VI) is about E^{ϕ}=1.1 V/Ag/AgCl [16, 24]. The $E_{BP\text{-}1}$ value within the range of ~1.09 to ~1.15 V of the investigated alloy steels (Table 2) falls near within the range of transpassive dissolution of Cr_2O_3 [Cr(III)] to chromate [Cr(VI)]. Hence, the $E_{BP\text{-}2}$ values at around of 1.59–1.7 V correspond to the beginning of the oxidation of the media (water). The 15 % Cr ODS steel with higher Cr showed marginally higher E_{BP} (1.62–1.73 V)

than 9 % Cr ODS (1.61–1.64 V) and follows by 11 % Cr F/M steel (1.59–1.63 V). In addition, the i_{pass} of 15 % Cr ODS steel is lower than 9 % Cr ODS and followed by 11 % Cr F/M steel (Table 2), but i_{pass} (1.5 V) of 15 % Cr ODS steel toward the $E_{BP\text{-}2}$ region is marginally higher than expected, and the reason is discussed later. Thus, based on the above observation it is plausible that the nitric acid concentration may differently impact the corrosion behavior of the investigated alloy steels.

The effects of nitric acid concentration on the corrosion resistance

The knowledge of the reduction process is essential to understand the corrosion of alloy steels in nitric acid, and cathodic dissolution of alloy steels takes place at potentials considerably lower than that at which hydrogen is discharged [24, 25]. Evans [16] described a basic mechanism that explains the autocatalytic reduction mechanism involved in nitric acid. Taking into account of the effects of nitric concentration, at high nitric acid concentration (>8 M HNO_3) or high temperature (>80 °C), the basic chemical reaction is the reduction of nitric acid to nitrous acid and nitrogen dioxide [16, 19, 20, 24, 25, 26].

$$2HNO_3 \rightarrow 2HNO_2 + O_2 \quad (1)$$

$$4HNO_3 \rightarrow 2H_2O + 4NO_2 + O_2 \quad (2)$$

For lower concentrations, the reduction of nitrous acid is the main electrochemical reaction, and the final products are NO [12, 19, 24, 26].

$$2HNO_2 \rightarrow NO_2 + NO + H_2O \quad (3)$$

The reduction of HNO_3 arises from the increase in the generation of the oxidant like NO_2, and its concentration increases when alloy steel corrodes [9, 20, 25].

$$Cr^{3+} + 2O_2 + 5e^- \rightarrow CrO_4^{2-} \quad (4)$$

The oxidant NO_2 produced in the above reactions is then adsorbed on the metal surface where it takes up an electron from dissolving metal to give NO_2^- anion [20, 24].

$$NO_2 + e^- \rightarrow NO_2^- \quad (5)$$

Furthermore, the presence of Y_2O_3 in passive film discussed later may not have a major influence in the corrosion process in nitric acid. The Y_2O_3 is a thermodynamically unstable oxide [5] and dissolves rapidly at low pH in nitric acid (high concentration). Hence, the presence of Y_2O_3 in the passive films may not have a significant benefit [5, 12]. The dominant corrosion reactions that are responsible for corrosion in nitric acid are the depolarizing cathodic reaction and the decomposition of unstable HNO_3 (Eqs. 1–4), that lead to a shift in the corrosion potential and transpassive corrosion [19, 20, 24]. The other factors attributed to the shift of corrosion potential in nitric acid are [9, 20, 25] (a) pure nitric acid–water solution, where the cathodic reaction is the

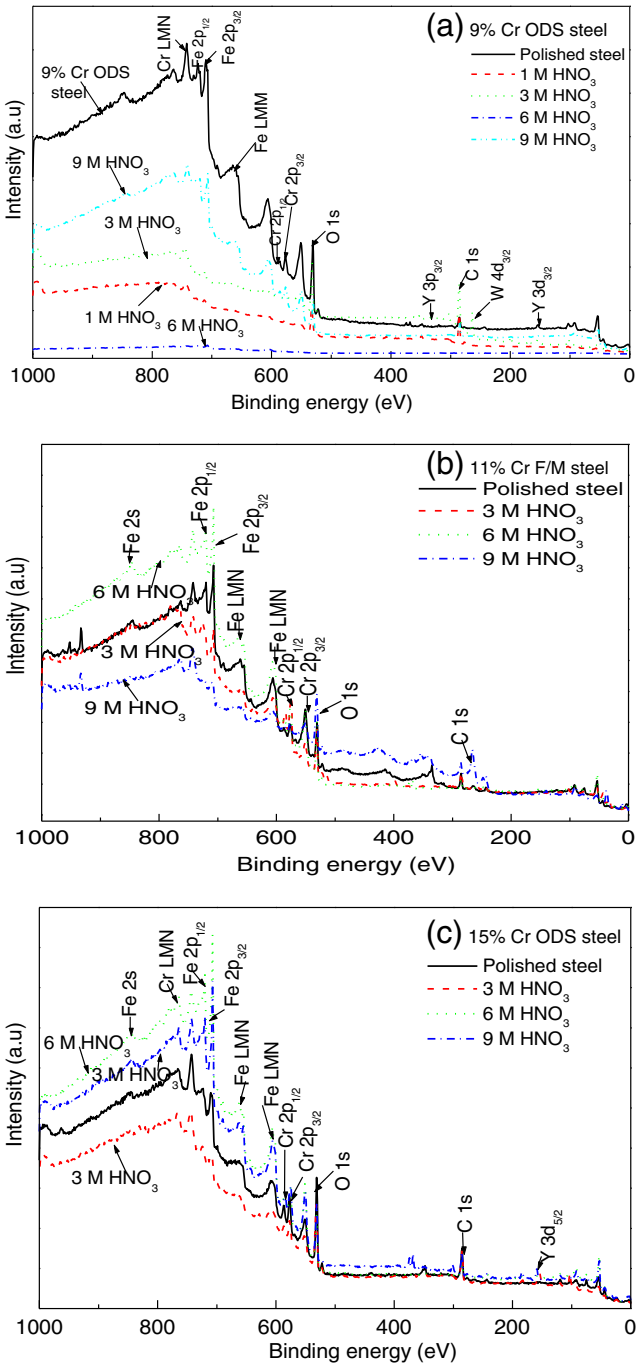

Fig 3 Surveyed spectrum of XPS measurements obtained for alloy steels in different nitric acid concentrations: **a** 9 % Cr ODS steel, **b** 11 % Cr F/M steel, and **c** 15 % Cr ODS steel

Table 3 The XPS measurements of different elements in atomic percent obtained in different nitric acid concentrations of alloy steels after polarization tests

Elemental concentration	Electrolytic solutions			
	(i)	(ii)	(iii)	(iv)
9 % Cr ODS steel				
Atomic percent	Fe=27.35	Fe=24.77	Fe=29.50	Fe=33.67
	Cr=9.52	Cr=19.95	Cr=14.92	Cr=13.98
	O=19.62	O=21.55	O=22.58	O=18.57
	Y=6.01	Y=6.26	Y=4.22	Y=4.91
11 % Cr F/M steel				
Atomic percent	Fe=27.28	Fe=16.45	Fe=15.55	Fe=17.88
	Cr=11.03	Cr=14.80	Cr=13.22	Cr=14.23
	O=22.62	O=20.75	O=23.50	O=24.94
15 % Cr ODS steel				
Atomic percent	Fe=27.10	Fe=24.08	Fe=31.50	Fe=33.70
	Cr=10.15	Cr=14.26	Cr=15.12	Cr=14.10
	O=20.51	O=21.80	O=19.56	O=18.45
	Y=5.77	Y=6.25	Y=6.21	Y=4.91

(i) Plain polished steel; (ii) 1 M HNO_3 (9 % Cr ODS steel) and 3 M HNO_3 (11 % Cr F/M and 15 % Cr ODS steels); (iii) 6 M HNO_3; (iv) 9 M HNO_3

reduction reaction of HNO_3; (b) nitric acid media containing oxidizing species; and (c) nitric media containing metallic elements electrochemically nobler, which causes galvanic coupling [19, 24]. In addition, with an increase in nitric acid concentrations, higher OCP (Fig. 1) and E_{corr} (Table 2) in 9 M HNO_3 may lead to more oxidizing nature and thereby increases the anodic dissolution (Figs. 2, Table 2). Subsequently, the increase in i_{pass} to the $E_{BP\text{-}2}$ region (Fig. 2) is also attributable to the highly oxidizing nature of solution that leads to less protective nature of the passive film. As a consequence, dissolution increases towards a higher anodic region followed by the oxidation of the media (water). Significantly, there is no trace of IGC for both ODS steels and in F/M steel even after the polarization test, thereby revealing good resistance to IGC. The presence of high density and uniformly dispersed fine particles in F/M steels and Y–Ti–O, Ti–O and Y_2O_3 particles in ODS steels [2, 3, 6, 7] may have a role in suppressing the IGC [4, 26]. In ODS steels, the uniform dispersion of nanosized particles (2–5 nm) within the metal matrix serves as a block for mobile dislocations to improve the high-temperature strength and act as a sink of point defects to maintain a resistance to radiation degradation [2, 7]. In addition, yttria in ODS steels also reduces the crystallite size and controls growth of grains through dispersion interaction [2, 7]. Thereby, microstructurally, the presence of such a high density and uniformly dispersed nanoclusters particles can suppress IGC and induce a beneficial effect. The possible IGC mechanism and the role of dispersed oxide have also been described elsewhere in our recent work [26]. Hence, it appears that the ODS steels suppresses IGC in nitric acid environment and pitting corrosion in some environment [4]. However, the exact mechanisms on how ODS steel suppresses IGC in nitric acid need more proper investigation.

The XPS analysis of the oxide films

The typical XPS surveyed spectra of passive film formed on 9 % Cr ODS, 11 % Cr F/M, and 15 % Cr ODS steels in different nitric acid concentrations are shown in Figs. 3a–c. The XPS spectra showed the presence of iron, chromium, oxygen, and carbon signals and yttrium, and tungsten was detected in ODS steels. To make clear the nature of the oxide film and the role of nitric acid, high-energy resolution spectra is collected for elements assigned in the survey spectra: iron (Fe 2p), chromium (Cr 2p), oxygen (O 1s), and yttrium (Y 2p and Y 3d). The corresponding atomic percent values are summarized in Table 3, and the carbon impurities that make up the balances of 100 % are not represented.

Typically, the Fe 2p spectra (Figs. 4a–c) showed two to three peaks at binding energy of ~706/707 eV, ~710 eV, and ~712 eV, corresponding to metallic Fe_{met}, Fe(III) oxide (Fe_2O_3), and Fe(III) hydroxide [$Fe(OH)_3$]. The 709.6 eV peak of Fe_3O_4 is not easily identifiable in the investigated alloy steels. The Fe 2p peak is broad, and the metallic substrate peak of Fe_{met} (~706.9 eV) is dominant in "as-received" air formed and in the film of polarized passive region (Fig. 4). This indicates that the film is thin. In addition, the metallic Fe peak positions are marginally shifted (Fig. 4), and these shifts in binding energy are attributed to ion etching/sputtering effects [12, 27, 28]. In 9 % Cr ODS steel (Fig. 4a), large peaks of Fe oxide (~27.35 at.%) observed in air-formed film diminished marginally (Table 3) and increased with nitric acid concentrations (24.77–33.70 at.%). In Fig. 4b, the Fe 2p of 11 % Cr F/M steel signal showed the presence of three components: metallic> Fe_{met} (~706 eV), Fe(III) oxide (~710 eV), and Fe(III) hydroxide (~712 eV). The Fe 2p spectra of 15 % Cr

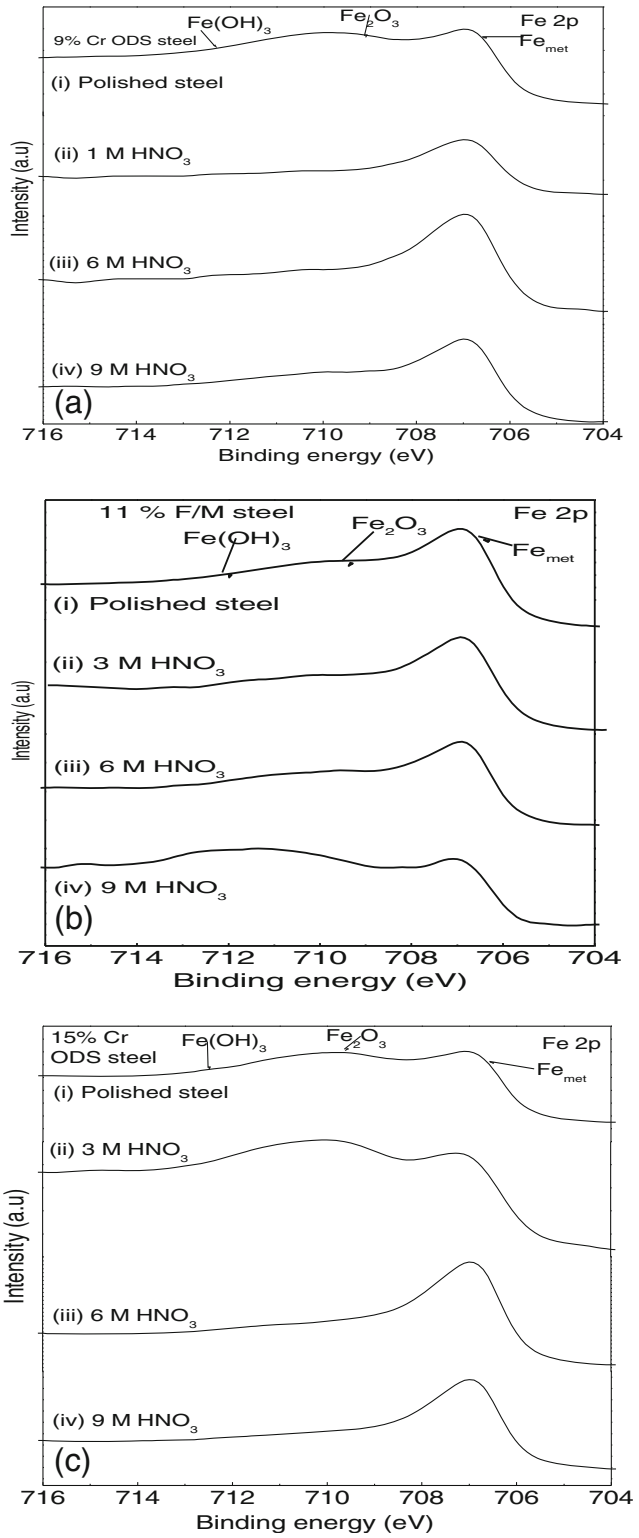

Fig 4 XPS spectra of Fe 2p detected for passive film formed on alloy steels in different nitric acid concentrations: **a** 9 % Cr ODS steel, **b** 11 % Cr F/M steel, and **c** 15 % Cr ODS steel

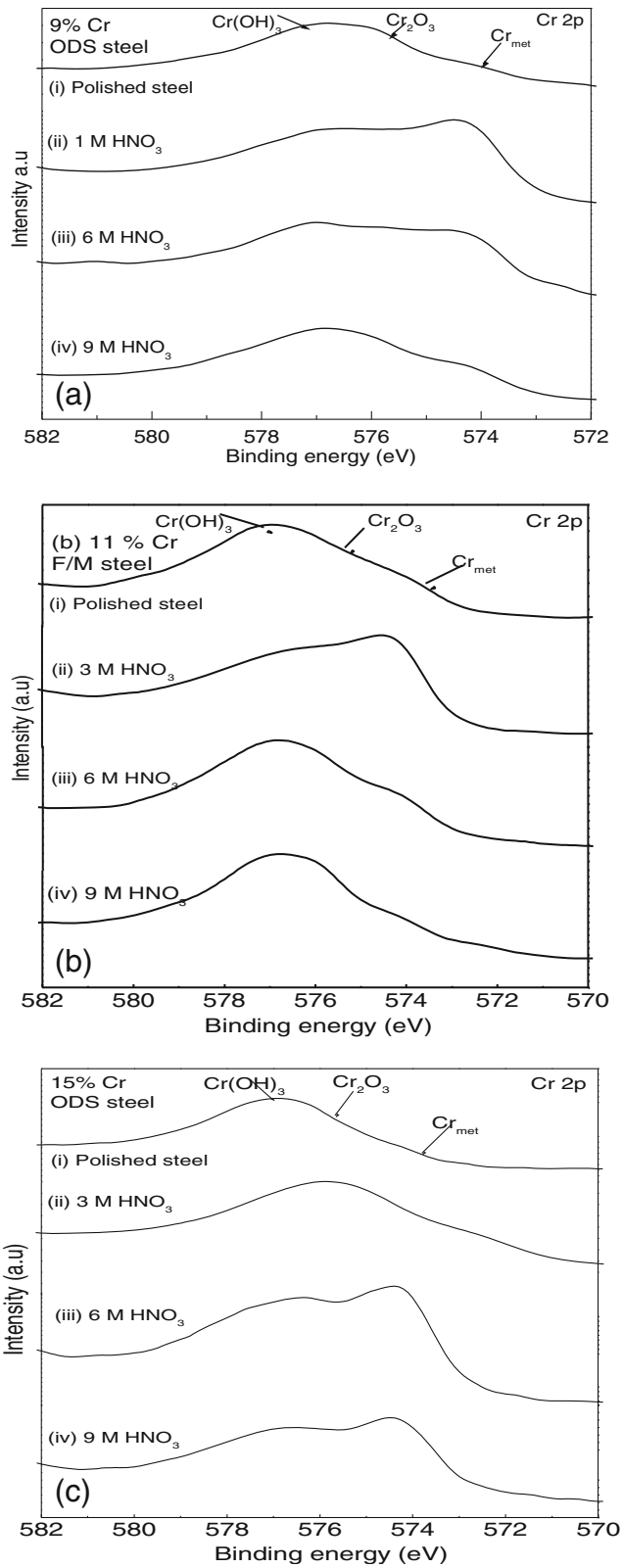

Fig 5 XPS spectra of Cr 2p detected for passive film formed on alloy steels in different nitric acid concentrations: **a** 9 % Cr ODS steel, **b** 11 % Cr F/M steel, and **c** 15 % Cr ODS steel

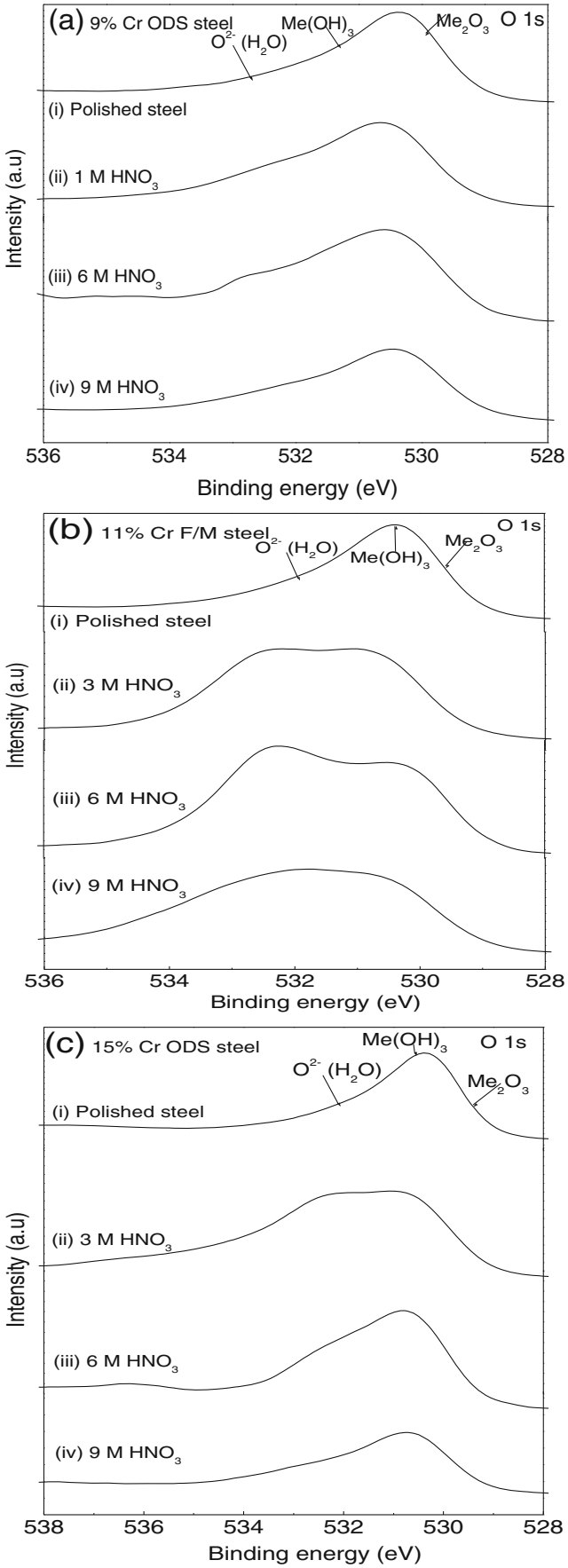

◀ **Fig 6** XPS spectra of O 1 s detected for passive film formed on alloy steels in different nitric acid concentrations: **a** 9 % Cr ODS steel, **b** 11 % Cr F/M steel, and **c** 15 % Cr ODS steel

ODS steel (Fig. 3c) is nearly same in shapes as observed in 9 % Cr ODS and 11 % Cr F/M steels, indicating the presence of oxidized and metallic state of iron. The passive oxide features agreed well with those presented in the literature [12, 28–30].

The high-resolution spectrums of Cr 2p in different nitric acid concentrations of the alloy steels are shown in Figs. 5a–c. The spectrum shows a broad distinct peak with a small shoulder related to Cr metal on the low-energy side. The Cr 2p ionization consisted mainly of three peaks in all the steels: The one at the lower binding energy (~574 eV) corresponds to metallic Cr_{met}, where the one at about ~576 eV are attributed to the presence of Cr(III) oxides and hydroxides (~577 eV). In air-formed film [Fig. 5a–c(i)], Cr_{met} (~574 eV) is not easily identifiable as masked by the other oxide constituents, but in passivated samples, the Cr metallic peaks are dominantly distinguishable with a broad hump. The presence of Cr(III) oxide (~576 eV) is prominently observed along with Cr(III) hydroxide (~577 eV). The corresponding binding

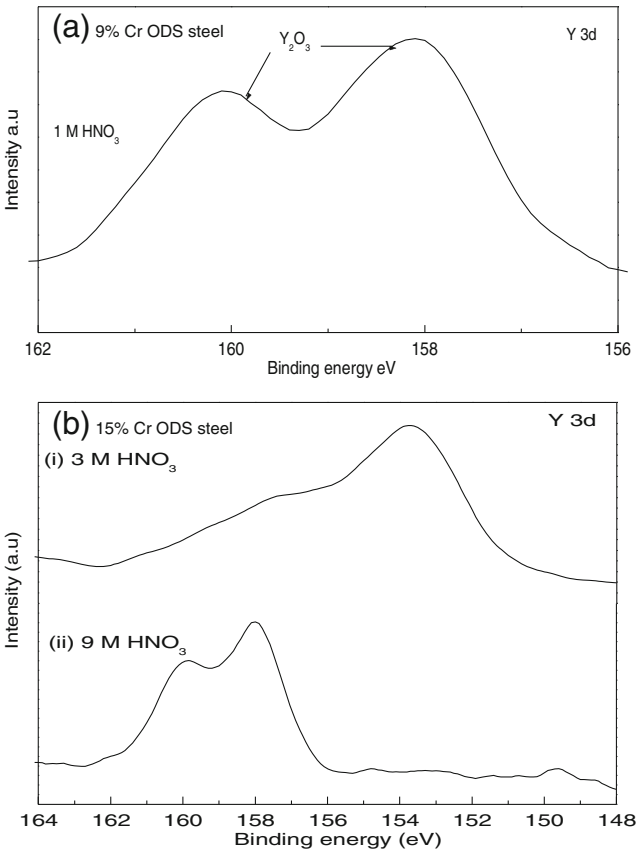

Fig 7 XPS spectra of Y 3d detected for passive film formed on alloy steels in different nitric acid concentrations: **a** 9 % Cr ODS steel and **b** 15 % Cr ODS steel

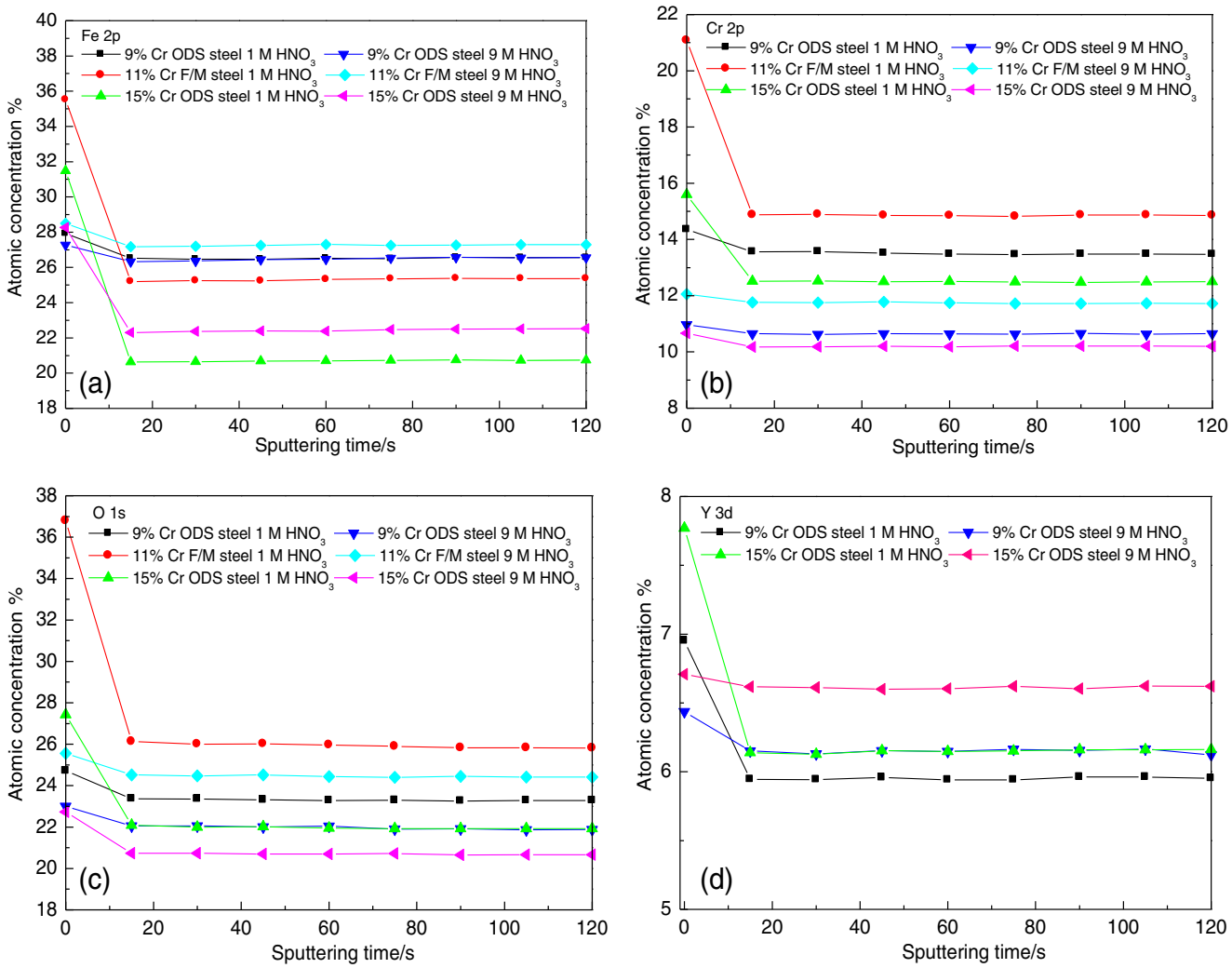

Fig 8 XPS depth profile (at.%) behavior of 9 % Cr ODS, 11 % Cr F/M and 15 % Cr ODS steels: **a** Fe 2p, **b** Cr 2p, **c** O 1 s, and **d** Y 3d obtained for different nitric acid concentrations

energies of Cr are in good agreement with the reported literature for passive films on Fe–Cr alloys [12, 26, 28, 30]. The relative proportion of the components (at.%) formed in the oxide film (Table 3) show that Cr is marginally enriched after polarization than air form films.

In Fig. 6a–c, the O 1 s spectra exhibit the oxygen features of three components: oxide, hydroxide and adsorbed H_2O. In all investigated alloy steel specimens, two peaks are detected at ~530 and ~531 eV, which were attributed to O^{2-} and OH^- attached to metal ions [26, 29], and third peak at ~532 eV originate from adsorbed H_2O. This could also show that oxygen peak consists of M–OH and M–O constituent peaks [12, 27]. The small shift of broad O 1 s signal (Fig. 6b and c) after passivation could also indicate the enrichment of adsorbed O^{2-} and OH^- [12, 27].

The XPS spectra of Y 3d of 9 % Cr ODS and 15 % Cr ODS steels are shown in Fig. 7a and b. The measured binding energy of ~158 and ~160 eV of Y 3d are consistent in the data reported for Y_2O_3 [12, 26, 29]. In Fig. 7a, Y 3d peak can be differentiated into two subpeaks of Y $3d_{5/2}$ and Y $3d_{3/2}$ for Y_2O_3 phase that appear at ~158 and ~160 eV, respectively. In 15 % Cr ODS steel in 3 M HNO_3, Y 3d peaks can be differentiated into two different subpeaks that appear at 152.7 and ~158 eV, whereas in 9 M HNO_3 [Fig. 7b(ii)], the Y 3d doublet binding energies at ~158 and 160 eV are assigned for Y $3d_{5/2}$ and Y $3d_{3/2}$ of the Y_2O_3 phase [12, 26].

Atomic concentration depth profile in different nitric acid concentrations

Figure 8 shows the sputter depth profiles of Fe 2p, Cr 2p, O 1 s, and Y 3d obtained for the 9 % Cr ODS, 11 % Cr F/M, and 15 % Cr ODS steels in different nitric acid concentrations. In Fig. 8a, the atomic percent of Fe content decreases during the initial stage of 15–20 s sputtering period, and Fe concentrations become constant with sputtering depth. In 9 % Cr ODS

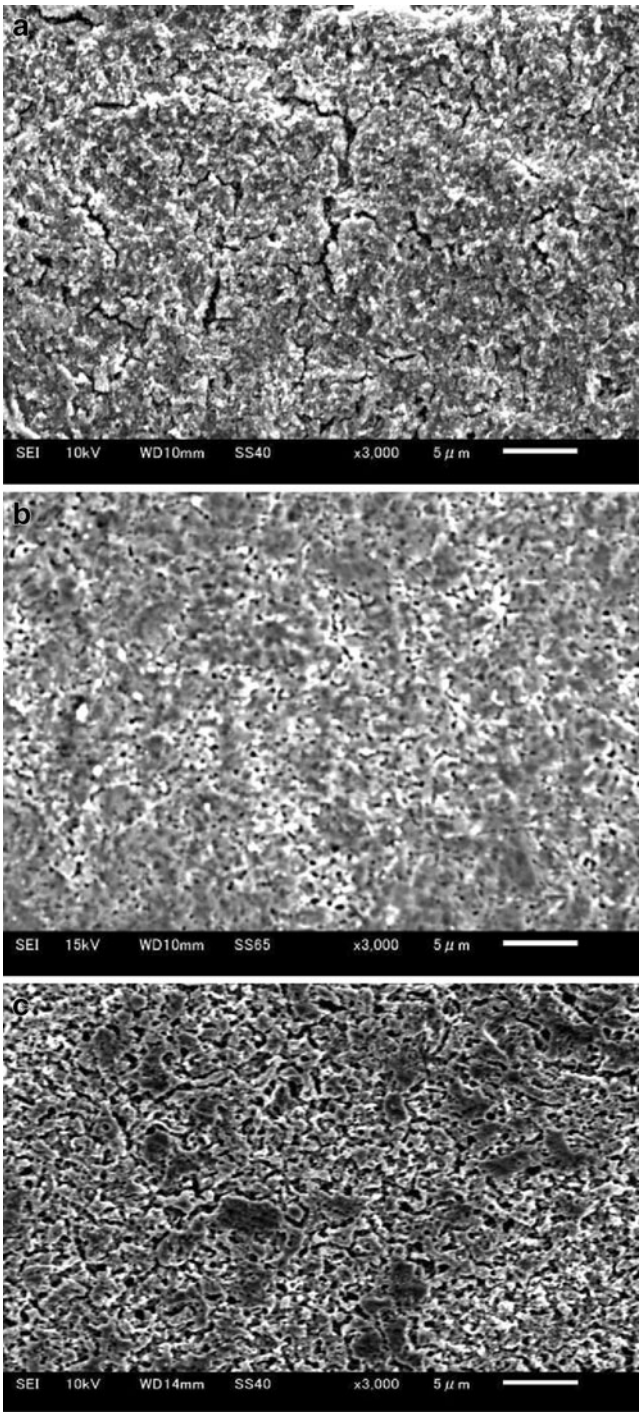

Fig 9 Typical SEM morphology of 9 % Cr ODS steel surface after potentiodynamic anodic polarization test: **a** 3 M HNO_3, **b** 6 M HNO_3, and **c** 9 M HNO_3

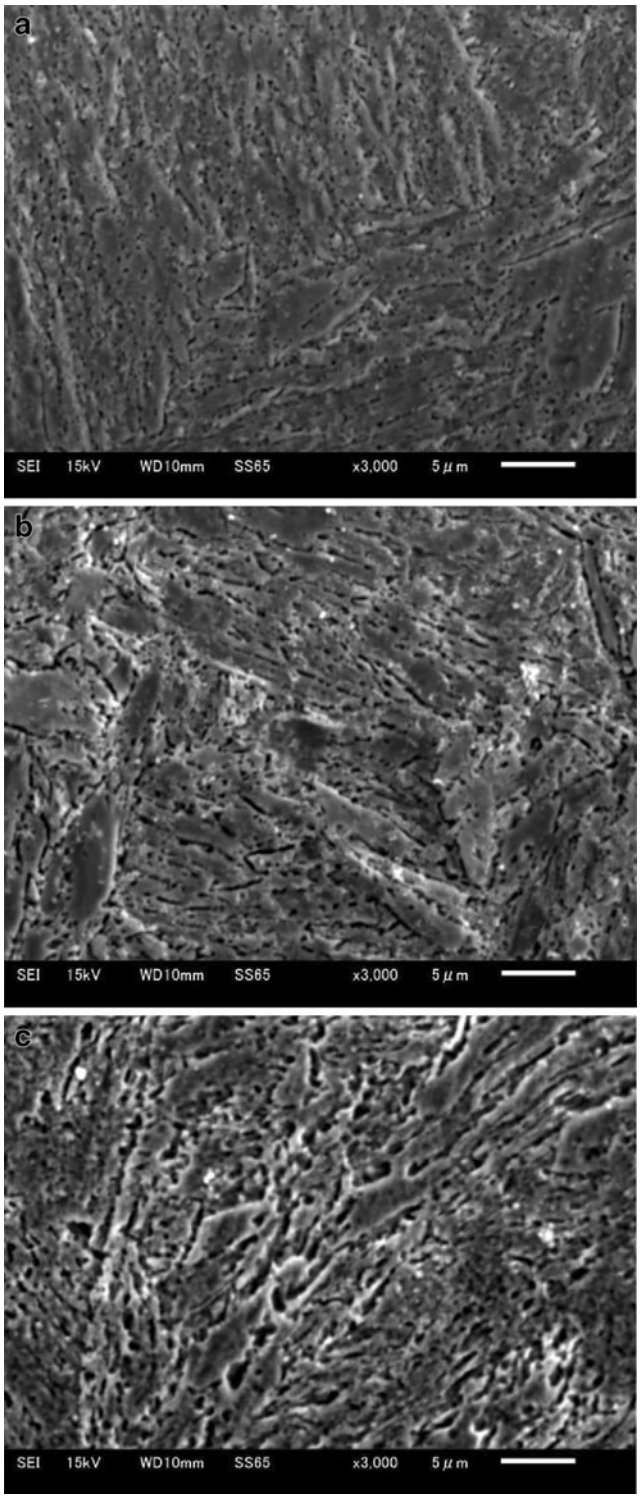

Fig 10 Typical SEM morphology of 11 % Cr F/M steel surface after potentiodynamic anodic polarization test in different nitric acid concentrations: **a** 3 M HNO_3, **b** 6 M HNO_3, and **c** 9 M HNO_3

steel (Fig. 8a), the Fe concentration in both 1 and 9 M HNO_3 is almost in the similar range. However, the concentration effects of nitric acid were seen in 11 % Cr F/M steel and 15 % Cr ODS steel. The higher Fe concentration in 9 % Cr ODS steel and 11 % F/M steels than 15 % Cr ODS steel is attributable to higher dissolution. In Fig 8b, the Cr atomic percent concentrations in the passive film were more in 1 M HNO_3

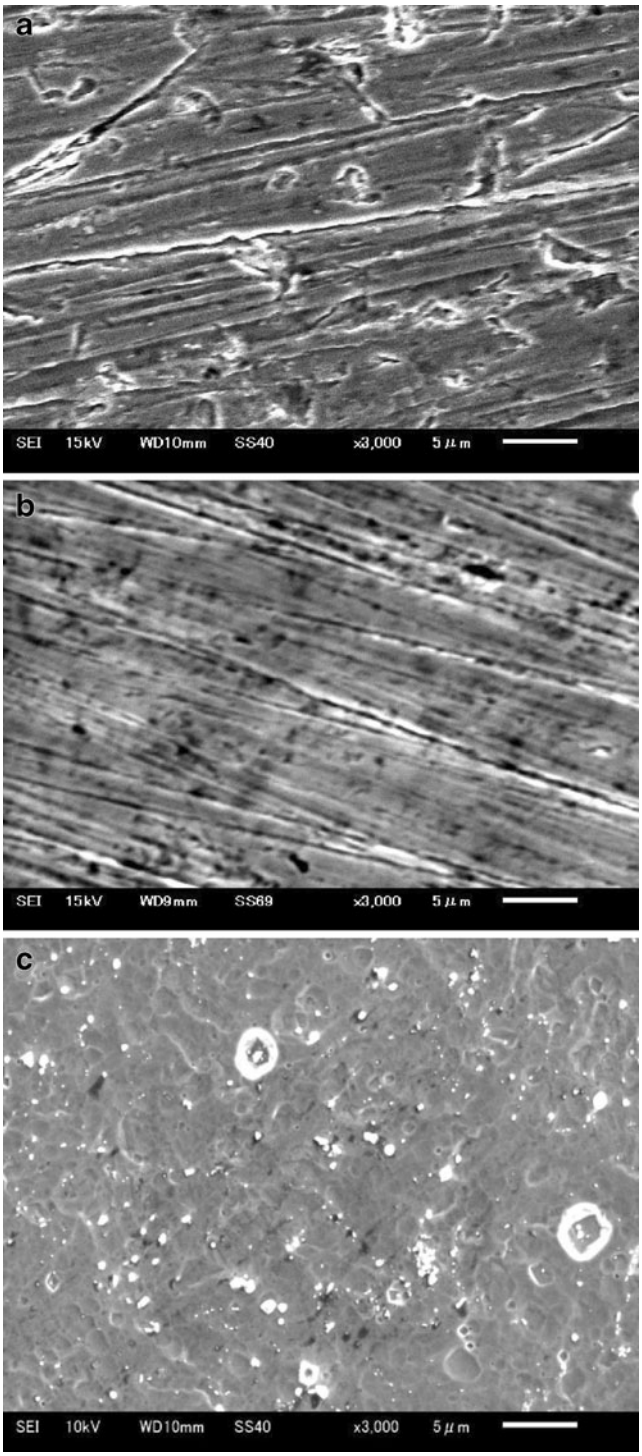

Fig 11 Typical SEM morphology of 15 % Cr ODS steel surface after potentiodynamic anodic polarization test in different nitric acid concentrations: **a** 3 M HNO_3, **b** 6 M HNO_3, and **c** 9 M HNO_3

than in 9 M HNO_3. The critical concentration of ~13 at.% Cr is necessary to confer passivity on binary Fe–Cr alloys. This could have a role in affecting on its corrosion resistance. In addition, the Fe and Cr atomic percent differences are seen between passive films formed under the OCP conditions (Fig. 8a) and those of passive film formed in the passive range (Table 3). Hence, it appears that the protecting properties of the passive layer at OCP conditions may be different from those of a film formed in the passive range. Similarly, although the chromium content in 15 % Cr ODS steel is higher than the one in 11 % Cr F/M and 9 % Cr ODS steels (Fig. 8b), the chromium concentration is marginally lower than the two alloy steels. Furthermore, the Fe and Cr concentrations are lower in both the nitric acid concentrations in 15 % Cr ODS steel attributed to lower dissolution. In higher 9 M HNO_3, the Cr seems to enrich (11 at.%) in the surface region, while the Cr content marginally decreases (to about 10 at.%) deeper into the surface. In the 9 % Cr ODS steel, an apparent concentration of ~12 at.% Cr is higher than the nominal alloy concentration of 9 % Cr. In both 9 % Cr ODS steel and 15 % Cr ODS steel, the Cr atomic percent is lower in higher 9 M HNO_3, indicating that chromium is not significantly enriched in the passive film, and kinetically less dissolved than iron. However, in those of passive film formed in the passive range (Table 3), the alloy steels showed marginally higher Cr content (14–20 at.% Cr) then in OCP conditions (Fig. 8). These could have arisen due to progressive increase in the area of the overlying oxide [31] and may have erred in detecting the metal signal and hence lower Cr is detected in 15 % Cr ODS steel. In addition, lower Cr content in higher nitric acid concentration may be one possible reason for the lower stability of the passive film of the alloy steels that show higher i_{pass} near $E_{BP\text{-}2}$ (Table 2). In addition, severe oxidizing environment in higher oxidizing potential could have led to more metal dissolution and offset the Cr role with a manifestation of higher i_{pass} near towards $E_{BP\text{-}2}$ (Table 2). The measured concentrations of oxygen Fig. 8c are in a similar range of the reported data [25, 32]. In 9 % Cr ODS and 15 % Cr ODS steels, Y is present within the range of ~6–7 at.% and notably, the dissolutions of elements are lower in 15 % Cr ODS steel than the other two alloy steels. The Y or Y_2O_3 found in the passive film and its influence on corrosion resistance in nitric acid needs more elaborate investigation.

In summary, judging by the OCP, anodic polarization, and XPS results, the optimum conditions for the oxide film stability are the Fe and Cr concentration in the passive film. As shown in Figs. 3, 4, 5, 6, and 7, the passive film has a mixture of mostly Cr_2O_3 and Fe_2O_3 in 11 % Cr steel and additionally Y_2O_3 in ODS steels. It is known that the electrochemical potential influences the chemical composition of

the passive oxide layer formed in the metal surface [15, 27, 28]. Similarly, the elemental profiles of Fe, Cr, and Y measured in OCP condition (Fig 8) and passive film formed in the passive range (Table 3) vary depending on the nitric acid concentration (Fig. 8). In addition, from the previously mentioned observations, the shift in OCP (Fig. 1), E_{corr} (Fig. 2), and increase of i_{pass} (Fig. 2) with increasing nitric concentration indicated that the stability of passive film was affected. This observation also suggests that the differences in nature, concentration, and change in the compositions of passive film in OCP condition (Fig. 8) and film formed in the passive range affected the corrosion resistance differently. This could be the plausible reason why lower Cr containing alloy steels exhibits higher Fe dissolution (Fig. 8a) leading to lower protective and lower corrosion resistance. However, further investigation with more elaborate investigation in nitric acid will be necessary to clarify such a correlation.

Surface morphology of the specimen after the corrosion test

The surface morphological features of the specimen after the corrosion test are shown in Figs. 9, 10, and 11, respectively. In Fig. 9, the surface morphology after polarization shows that the oxide layer formed in 9 % Cr ODS steel has cracks, porous and pore-like network structure. In Fig. 10, the F/M steel surface revealed similar features of high pores network in all the nitric acid concentrations. The surface morphologies of the specimen after polarization of 15 % Cr ODS steel shown in Fig. 11 are different. The surface does not show any pore layer formation, but changes in surface morphology with small pits shape dissolution were noticed at higher nitric acid concentration. However, as mentioned earlier all the investigated alloy steels even after the polarization test does not show any intergranular corrosion attack. This could be attributed to the role of homogenously distributed nanosized dispersed oxide [26] that improved IGC resistance in the studied nitric acid concentration. IGC is a problem associated with most austenitic grade stainless steels used in PUREX reprocessing application [8, 9, 19, 20]. Hence, from a practical point of view resistance to IGC induced, degradation is important to the structural materials to be used in nitric acid production and spent nuclear fuel reprocessing plants [5, 8, 19, 24].

Conclusions

The corrosion resistance, passive film compositions, and the surface morphology of F/M and ODS steels for applications in different nitric acid media are evaluated. The influences of nitric acid concentrations show that the shift of open circuit potential towards noble potential was more in 9 % Cr ODS steel and 11 % Cr F/M steel than in the 15 % Cr ODS steel. This shift is undesirable due to highly oxidizing nature at higher nitric concentration. Similarly, the nitric acid concentration differently impacts the corrosion behavior of the alloy steels as evident from the potentiodynamic polarization measurements. The 15 % Cr ODS steel exhibited lower corrosion potential and passive current density, and a marginally higher breakdown potential than 11 % Cr F/M and 9 % Cr ODS steels. The XPS analysis of the oxide formed is composed predominantly of Fe_2O_3 along with Cr_2O_3 and Y_2O_3 depending on alloy composition. Higher Cr concentrations in the passive film were noticed than in the air-formed film. The depth profiles of the passive film at OCP condition show that the Cr concentration in the passive film was more in 1 M HNO_3 than in 9 M HNO_3. The Fe and Cr concentration in the passive film of 15 % Cr ODS steel is marginally lower than the two other alloy steels. This may be one reason for the lower stability of the passive film of 15 % Cr ODS steel that showed higher passive current density near breakdown potential. The SEM of the surface morphology shows porous oxide layers in 9 % Cr ODS and 11 % Cr F/M steels than almost none in 15 % Cr ODS steel. All the investigated alloy steels do not show any intergranular corrosion attack thereby revealing good resistance to nitric acid in the studied concentrations. Hence, from a practical point of view, this may be desirable for the structural materials to be used in a nuclear reprocessing plant.

Acknowledgments One author, Dr S.N., gratefully acknowledged Japan Society for the Promotion of Science, Tokyo, Japan for the postdoctoral fellowship and financial support.

References

1. Ukai S, Fujiwara M (2002) Perspective of ODS alloys application in nuclear environments. J Nuclear Mater 307–311:749–757
2. Ukai S (2012) Oxide dispersion strengthened steels. Comp Nuclear Mater 4:241–271
3. Baluc N, Abe K, Boutard JL, Chernov VM, Diegele E, Jitsukawa S, Kimura A, Klueh RL, Kohyama A, Kurtz RJ, Lässer R, Matsui H, Möslang A, Muroga T, Odette GR, Tran MQ, van der Schaaf B, Wu Y, Yu J, Zinkle SJ (2007) Status of R&D activities on materials for fusion power reactors. Nuclear Fus 47:S4696
4. Isselin J, Kasada R, Kimura A (2011) Effects of aluminum on the corrosion behavior of 16 % Cr ODS ferritic steels in a nitric acid solution. J Nuclear Sci Tech 48:169–171
5. Gwinner B, Auroy M, Mas D, Saint-Jevin A, Pasquier-Tilliette S (2012) Impact of the use of the ferritic/martensitic ODS steels cladding on the fuel reprocessing PUREX process. J Nuclear Mater 428:110–116
6. Yvon P, Carré F (2009) Structural materials challenges for advanced reactor systems. J Nuclear Mater 385:217–222
7. Lindau R, Möslang A, Rieth M, Klimiankou M, Materna-Morris E, Alamo A, Tavassoli A-AF, Cayron C, Lancha A-M, Fernandez P, Baluc N, Schäublin R, Diegele E, Filacchioni G, Rensman JW,

Schaaf BVD, Lucon E, Dietz W (2005) Present development status of EUROFER and ODS-EUROFER for application in blanket concepts. Fus Engin Design 75–79:989–996
8. Raj B, Kamachi Mudali U (2006) Materials development and corrosion problems in nuclear fuel reprocessing plants. Prog Nuclear Energy 48:283–313
9. Ningshen S, Kamachi Mudali U, Ramya S, Raj B (2011) Corrosion behaviour of AISI type 304L stainless steel in nitric acid media containing oxidizing species. Corrosion Sci 53:64–70
10. Allen TR, Chen Y, Ren X, Sridharan K, Tan L, Was GS, West E, Guzonas D (2012) Material performance in supercritical water. Comp Nuclear Mater 5:279–326
11. Huét JJ, Leroy V (1974) Dispersion strengthened ferritic steels as fast reactor structural materials. Nucl Tech 24:216-224
12. Ningshen S, Sakairi M, Suzuki K, Ukai S (2013) The passive film characterization and anodic polarization behavior of 11 % Cr ferritic/martensitic and 15 % Cr oxide dispersion strengthened steels in different electrolytic solutions. Applied Surface Sci 248:345–355
13. Ningshen S, Sakairi M, Suzuki K, Ukai S (2012) Corrosion resistance and passive film characterization of 9Cr oxide dispersion strengthened steel in acidic and chloride environment. Proc. 6th. Japan–China Joint Seminar on Marine Corrosion, Tokyo, Japan, pp. 7–17
14. Marcus P, Olefjord I (1988) A round robin on combined electrochemical and AES ESCA characterization of the passive films on Fe-Cr and Fe-Cr-Mo alloys. Corros Sci 28:589–602
15. Sugimoto K (2008) Passive films on stainless steels: present state of analysis and understanding. Zairyo-to-Kankyo 57:375–384
16. Evans UR (1960) The corrosion and oxidation of metals. Edward Arnold, London
17. Kolman DG, Ford DK, Butt DP, Nelson TO (1997) Corrosion of 304 stainless steel exposed to nitric acid-chloride environments. Corros Sci 39:2067–2093
18. Wagner CW, Traud W (1938) Über die Deutung von Korrosionsvorgängen durch Überlagerung von Electrochemischen Teilvorgängen und über die Potentialbildung an Mischelektroden. Z Elektrochem 44:391–402
19. Whillock GOH, Worthington SE (2010) Corrosion in nitric acid. In: Richardson TJA, Cottis BRA, Lindsay R, Lyon S, Scantlebury DJD, Stott H, Graham M (eds) Shreir's corrosion, vol 2. Elsevier, Amsterdam, pp 1250–1269
20. Kiuchi K, Hayashi M, Hayakawa H, Sakairi M, Kikuchi M, (1991) Proceedings of Third International Conference on Nuclear fuel Reprocessing and Waste Management, (RECOD-91), vol. 2. Sendai, Japan, pp. 549–554
21. Sato N (1982) Anodic breakdown of passive films on metals. J Electrochem Soc 129:255–260
22. Macdonald DD (1992) The point defect model for the passive state. J Electrochem Soc 139:3434–3449
23. Betova I, Bojinov M, Laitinen T, Mäkelä K, Pohjanne P, Saario T (2002) The transpassive dissolution mechanism of highly alloyed stainless steels - I. Experimental results and modelling procedure. Corros Sci 44:2675–2697
24. Fauvet P, Balbaud F, Robin R, Tran QT, Mugnier A, Espinoux D (2008) Tran QT, Mugnier A, Espinoux D (2008) Corrosion mechanisms of austenitic stainless steels in nitric media used in reprocessing plants. J Nuclear Mater 375:52–64
25. Balbaud F, Sanchez G, Fauvet P, Santarini G, Picard G (2000) Mechanism of corrosion of AISI 304L stainless steel in the presence of nitric acid condensates. Corrosion Sci 42:1685–1707
26. Ningshen S, Sakairi M, Suzuki K, Ukai S (2013) Corrosion resistance behavior of 9 % Cr oxide dispersion strengthened steel in different electrolytic media. Corrosion. doi:10.5006/0839
27. Keller P, Strehblow H (2004) XPS investigations of electrochemically formed passive layers on Fe/Cr-alloys in 0.5 M H2SO4. Corrosion Sci 46:1939–1952
28. Olsson C-OA, Landolt D (2003) Passive films on stainless steels-chemistry, structure and growth. Electrochim Acta 48:1093–1104
29. Handbook of X-ray photoelectron spectroscopy (1991) JEOL, Tokyo
30. Asami K, Hashimoto K, Shimodaira S (1978) An XPS study of the passivity of a series of iron-chromium alloys in sulphuric acid. Corrosion Sci 18:151–160
31. Castle JE, Clayton CR (1977) The use of in the x-ray photo-electron spectroscopy analyses of passive layers on stainless steel. Corros Sci 17:7–26
32. Liu CT, Wu JK (2007) Influence of pH on the passivation behavior of 254SMO stainless steel in 3.5 % NaCl solution. Corrosion Sci 49:2198–2209